Materials Advances

ROYAL SOCIETY OF CHEMISTRY

PAPER

View Article Online
View Journal | View Issue

Cite this: *Mater. Adv.*, 2022, 3, 8351

Optimization of spray-coated nanochitin/nanocellulose films as renewable oxygen barrier layers *via* thermal treatment†

Yue Ji, [a] D. Eric Shen, [bc] Elizabeth K. Young,[d] Callie L. Goins, [b] John R. Reynolds, [bcd] Meisha L. Shofner [de] and J. Carson Meredith *[ae]

The demand for food and pharmaceutical packaging materials is increasing, but the most common materials used are non-renewable, non-biodegradable petroleum-based plastics, which has resulted in many end-of-life problems. Cellulose nanocrystals (CNCs) and chitin nanowhiskers (ChNWs) have high strength and low oxygen permeability (OP), providing a renewable alternative. In this work, we spray coated ChNWs and CNCs on cellulose acetate (CA) film and tuned the film properties by adjusting the spray coating temperature (T_{spray}) and the post thermal treatment temperature ($T_{thermal}$). Importantly, by increasing T_{spray} (from 40 to 100 °C) and $T_{thermal}$ (from 40 to 140 °C), the OP decreased 48% and 62%, respectively. The optimal OP (*i.e.*, 11.5 cm^3 μm m^{-2} day^{-1} kPa^{-1}) is comparable to that of commercial oriented poly(ethylene terephthalate). Film transmittance and haze were dependent on both temperatures, with higher T_{spray} and $T_{thermal}$ giving rise to coated films with lower haze and higher transmittance values approaching those of bare CA. The mechanical properties and water vapor barrier properties of the coated films were on average 20% and 11% enhanced compared to neat CA, without being significantly influenced by the temperatures. These properties support the use of the polysaccharide-based film as a renewable substitute in packaging applications.

Received 18th July 2022,
Accepted 21st September 2022

DOI: 10.1039/d2ma00832g

rsc.li/materials-advances

Introduction

Barrier packaging materials, which are used to protect food and pharmaceuticals from deterioration, contamination, and damage, are playing an increasingly significant role in modern life.[1] These materials often require low gas permeabilities, especially for oxygen and moisture, mechanical integrity, and in some cases high optical transparency for customers to clearly see the product.[2]

Common materials for barrier packaging include layers consisting of metal films, plastics, and paper materials.[1] Among them, plastics are the most used materials for food and beverage packaging, and ~50% of Europe's food is packed in layered plastics, consisting often of poly(ethylene terephthalate) (PET), polyolefins, poly(vinyl chloride) (PVC), polyamide, and ethylene vinyl alcohol (EVOH), *etc.*[3] However, these are petroleum-based materials, which are non-renewable, non-biodegradable and are not recycled. It takes decades to thousands of years for them to degrade, which has resulted in widescale pollution in the ocean and soil.[4] Though some PET and polyolefins are synthesized from renewable sources, the end-of-life problems caused by their non-biodegradability still exist.[5] Only limited types of bio-based, biodegradable materials have been commercialized as gas barriers in food packaging, such as starch, cellophane, poly(lactic acid) (PLA), and poly(hydroxyalkanoates) (PHAs).[1]

Cellulose and chitin, as the first and second most abundant polysaccharides in nature, have gained attention for packaging applications.[6] Cellulose is a homopolymer of D-glucose, and chitin consists of *N*-acetyl-D-glucosamine units. Because of strong intermolecular hydrogen bonding, cellulose and chitin have high crystallinity, and their nanomaterials have high modulus and strength as well as low oxygen permeabilities (OP).[7,8] These nanomaterials include cellulose nanofibrils (CNFs),[9] cellulose nanocrystals (CNCs),[10] chitin nanofibers (ChNFs),[10,11] chitin nanocrystals,[12] and chitin nanowhiskers (ChNWs).[13]

[a] *School of Chemical & Biomolecular Engineering, Georgia Institute of Technology, Atlanta, GA 30332, USA. E-mail: carson.meredith@chbe.gatech.edu*
[b] *School of Chemistry and Biochemistry, Georgia Institute of Technology, Atlanta, GA 30332, USA*
[c] *Center for Organic Photonics and Electronics, Georgia Tech Polymer Network, Georgia Institute of Technology, Atlanta, GA 30332, USA*
[d] *School of Materials Science and Engineering, Georgia Institute of Technology, Atlanta, GA 30332, USA*
[e] *Renewable Bioproducts Institute, Georgia Institute of Technology, Atlanta, GA 30332, USA*

† Electronic supplementary information (ESI) available. See DOI: https://doi.org/10.1039/d2ma00832g

They can be applied as fillers in a matrix, as free-standing films, or as coatings on a substrate to form an oxygen barrier by forming a densely packed tortuous structure where the pathway for O_2 transport is elongated.[6] However, when they are blended with another material, the biodegradability can be limited.[14] Besides, thick free-standing films of CNCs, ChNFs, and ChNWs are usually brittle and may require plasticizer to satisfy requirements of mechanical properties for food packaging applications.[10,15,16] Additionally, this approach utilizes larger amounts of material than are required to obtain the desired barrier properties. Thus, an attractive approach to use nanocellulose or nanochitin for sustainable packaging is to apply them as thin layers on a substrate that provides mechanical support.[17,18]

Previous studies have shown that nanocellulose and nanochitin can be applied in sequence as multilayer coatings to form an excellent oxygen barrier.[19–23] Because chitin nanomaterials are usually partially deacetylated during extraction, they are positively charged in acidic media due to protonated amino groups. Cellulose nanomaterials, in contrast, are usually negatively charged during (2,2,6,6-tetramethylpiperidin-1-yl)-oxyl- (TEMPO-) oxidation (for CNFs) or hydrolysis with sulfuric acid (for CNCs from pulp). When they are applied as a multilayer coating, the electrostatic attraction between nanocellulose and nanochitin can facilitate the formation of a dense interface and result in enhanced gas barrier properties. For instance, we have reported in previous literature that cellulose acetate (CA) coated with a bilayer of ChNWs and CNCs demonstrated up to 66% and 85% lower oxygen permeabilities than CA films coated with a single layer of ChNFs or CNCs, respectively.[22] Similar results have also been reported for PLA coated with five alternating ChNF and CNC layers and PET coated with up to 40 alternating layers of chitosan nanowhiskers (CsWs) and CNFs (chitosan is highly deacetylated chitin).[20,23] However, in many reports of nanochitin and nanocellulose multilayer coatings, usually more than ten alternating layers are applied.[19–21,24] This may increase the cost and complexity of their scale-up production compared to bilayer coatings. Thus, optimizing the properties of a film coated with only one bilayer of nanochitin and nanocellulose would be important for improving the practical feasibility of the technology.

A simple way to improve the gas barrier properties is thermal annealing. It has been reported that thermally treating a free-standing film of TEMPO-oxidized CNF at a temperature greater than 100 °C decreases its OP and water vapor permeability.[9,25] Hot pressing at 80 °C can also improve the oxygen barrier property of a PET film coated with ChNWs, CNFs, or their multilayers.[20] Nevertheless, it remains unclear how thermal treatment will influence the microstructure and properties of a ChNW–CNC bilayer-coated film.

In this work, we optimized for the first time the gas barrier properties of a polysaccharide-based multilayer film through straightforward control of the coating and annealing temperatures. Using CA as the substrate, suspensions of ChNWs and CNCs were spray-coated on top in sequence at varying temperatures (T_{spray}) to form a dry gas barrier, followed by placing the films in an oven at varying thermal annealing temperatures ($T_{thermal}$). The influences of T_{spray} and $T_{thermal}$ on the microstructure of the multilayer film and the optical, mechanical, and oxygen and water vapor barrier properties were studied, affording highly transparent and mechanically robust materials with OP of 11.5 ± 0.9 cm^3 μm m^{-2} day^{-1} kPa^{-1}. This demonstrates a simple and effective procedure to produce renewable films with competitive barrier properties that could address end-of-life accumulation challenges caused by commercially available but non-renewable alternatives.

Experimental methods

Materials

The CA substrates were purchased from Goodfellow Cambridge Ltd, USA. A 0.5 wt% ChNW suspension was obtained by deacetylating commercial chitin (Tidal Vision, USA) sourced from crustacean shells under the optimized conditions as previously reported, *i.e.*, in a 40% sodium hydroxide (NaOH) solution heated with an oil bath at 155 °C for 140 min with a liquid–solid ratio of 25 : 1 (mL g^{-1}), followed by high-pressure homogenization.[22] A 0.5 wt% CNC suspension was obtained by diluting a 10 wt% CNC slurry extracted from pulp provided by USDA Forest Products Laboratory, USA. The properties for CA, ChNW, and CNC are available in Tables S1, S2 and S3 (ESI†) respectively, and details about their characterizations are available in the ESI.† NaOH, acetic acid, and magnesium nitrate ($Mg(NO_3)_2$) were purchased from Sigma-Aldrich, USA.

Spray coating and thermal treatment

The spray coating setup is shown in Fig. S1 (ESI†). A gravity-fed spray gun with a 1.4 mm nozzle (PNTGREEN, USA) was connected to a liquid reservoir containing the ChNW or CNC suspension. N_2 was supplied as a carrier gas at 40 psi. During the coating process, the CA film was fixed to a hot plate maintained at a controlled temperature (T_{spray}) by using tape to seal its edges, and the spray nozzle was kept ~20 cm away from the heated surface. A volume of 25 mL of 0.5 wt% ChNW or 25 mL of 0.5 wt% CNC was spray-coated on 7.5″ × 7.5″ CA film in sequence. Between subsequent sprays, the sprayed liquid was dried for 2 min. The spraying operation was done in a fume hood. After the coating was dried, the coated film was exposed to the room atmosphere (~50% RH) for one day and then conditioned at ~53% RH in a sealed container with saturated $Mg(NO_3)_2$ solution used to regulate and maintain the RH at room temperature for 7 days. The resulting film was placed in an oven at a controlled temperature ($T_{thermal}$) for 1 hour and then conditioned at 50% RH at room temperature for at least 7 days before characterization.

For the optimization of the film properties, the T_{spray} and $T_{thermal}$ were tuned. The T_{spray} varied from 40 to 100 °C; the lower limit was selected to ensure films dried within a reasonable time (*i.e.*, 2 minutes at 40 °C) while the upper limit was selected as films sprayed at higher temperatures became noticeably yellow. The $T_{thermal}$ ranged from 40 to 140 °C, with

Table 1 Preparation temperatures and thicknesses for untreated CA and coated samples

Sample	Thickness (μm)	T_{spray} (°C)	$T_{thermal}$ (°C)
CA	76 ± 1	—	—
S40T40	79 ± 1	40	40
S60T40	79 ± 2	60	40
S80T40	80 ± 1	80	40
S100T40	79 ± 1	100	40
S80T*n*	79 ± 1	80	—
S80T60	79 ± 1	80	60
S80T80	80 ± 2	80	80
S80T100	80 ± 1	80	100
S80T120	79 ± 1	80	120
S80T140	79 ± 1	80	140

an upper limit of 140 °C determined from previous work on cellulose nanofibril films optimized for oxygen and moisture barrier performance.[9] The resulting coated CA film is referred to as ST_{spray}T$T_{thermal}$. For instance, a film spray-coated at 80 °C and thermally treated at 40 °C is designated S80T40. A control sample spray-coated at 80 °C without further thermal treatment is referred to as S80T*n*. The preparation conditions for coated CA films are summarized in Table 1. Two other sample sets were prepared for comparison: (1) CAST_{spray} sample sets that were CA substrates spray-coated with 50 mL of deionized water at a controlled T_{spray} ranging from 40 to 100 °C (*i.e.*, CAS40 to CAS100), and (2) CAT$T_{thermal}$ sample sets that were uncoated CA substrates thermally treated at a controlled $T_{thermal}$ ranging from 40 to 140 °C (*i.e.*, CAT40 to CAT140).

Characterization

The thickness and the cross-sectional structure for the ChNW–CNC coating were obtained by scanning electron microscopy (SEM; SU8010, Hitachi High-Tech Corp., Japan) as previously reported.[22] The thicknesses were calculated from SEM based on the known thickness for CA (76 ± 1 μm). The oxygen permeability (OP) of a coated film was measured by using a Class 230 Oxygen Transmission Rate Test System (Labthink International, Inc., USA) at 23 °C and 50% relative humidity (RH) for the O_2 feed side, which the coating was exposed to, and 0% RH for the N_2 side. The water vapor transmission rate (WVTR) was measured by a PERMATRAN-W 1/50 instrument (MOCON, USA) at 23 °C and 50% RH for the permeant side and 5% RH for the dry side, which the coating was exposed to. The water contact angle on the uncoated CA and the CNC side of the coated films was measured by a goniometer (Model 290, Ramé-hart instruments co., USA). The ChNW–CNC coating was peeled off from the substrate and subject to thermogravimetric analysis (TGA; TGA2, Mettler Toledo, USA) to obtain the moisture content of the coating. In this experiment, the samples were heated from 40 to 200 °C at a rate of 10 °C min^{-1} under 20 mL min^{-1} N_2 flow, and the moisture content was calculated as the mass loss percentage from 40 to 180 °C. Densities of selected coated films and the untreated CA film were measured by displacement (ASTM D792) in triplicate, by using isopropanol instead of deionized water to avoid influences on the coating.

The mechanical properties of the films were measured by a universal testing system (INSTRON 5566, USA) utilizing a 100 N load cell. The modulus, ultimate tensile strength, and failure strain were obtained by utilizing microtensile testing (ASTM D1708) at a crosshead speed of 1 mm min^{-1}, and the breaking force was obtained using puncture testing (ASTM F1306) at a crosshead speed of 25 mm min^{-1}. For each treated film, 4 specimens were tested in the microtensile testing and 3 specimens were tested in the puncture testing. For untreated CA film, both tests were replicated 5 times.

The light transmittance spectrum was measured using a Cary 5000 spectrophotometer, and haze was measured using an integrating sphere (DRA 2500) by following ASTM D1003. The surface roughness was measured by profilometry using a DektakXT profilometer (Bruker, UK) with a scan rate of 20 μm s^{-1} and a force of 3 mg. Film morphology was characterized using an BX51 microscope (Olympus, Japan) in transmission mode using 10× magnification.

Results and discussion

Microstructure of the coating

The coated CA films were obtained by spray coating first ChNW, and then CNC, on the CA substrate in sequence, followed by thermal treatment, as shown in Fig. 1a. The resulting coated CA films had a total thickness of 79–80 μm (Table 1), where the CA substrate had a thickness of 76 ± 1 μm and the ChNW–CNC bilayer coating thickness was 3–4 μm, as shown in Fig. 1b. The coating consists of piled lamellae of ChNWs and CNCs, and no visible boundary was observed between these two layers, as shown in Fig. 1c. The T_{spray} and $T_{thermal}$ did not significantly influence the microstructure of the coating, as shown in cross-sectional SEM images in Fig. S2 (ESI†).

Oxygen barrier property

The coating of ChNW and CNC formed an efficient oxygen barrier on the CA substrate, and the OP of coated films significantly decreased by increasing the T_{spray} and the $T_{thermal}$. As shown in Fig. 2, by increasing the T_{spray} from 40 to 100 °C at a controlled $T_{thermal}$ of 40 °C, the OP of the coated film decreased from 44.3 ± 1.3 to 23.3 ± 3.9 cm^3 μm m^{-2} day^{-1} kPa^{-1}. As a comparison, the OP of a treated CA film was not significantly influenced by increasing the T_{spray} and the $T_{thermal}$ (Table S4, ESI†) and was on average 535 ± 38 cm^3 μm m^{-2} day^{-1} kPa^{-1}. Because the ChNW–CNC coating is controlling the OP of the coated film, the small influences of T_{spray} and $T_{thermal}$ on the OP of the CA substrate are not significant to the overall structure's OP.[26] The decrease in OP of S40T40 to S100T40 is probably attributed to the decrease in the moisture content in the ChNW–CNC coating from 5.2 ± 1.2 to 4.4 ± 0.9%, although this decrease was within the error bars, as is shown in Fig. S3a (ESI†). The decrease in moisture content with an increasing T_{spray} may be the result of an increasing degree of hornification, *i.e.*, a decreasing capacity to hold free moisture due to fiber aggregation during solvent evaporation at increasingly elevated T_{spray}.[27] A higher equilibrium moisture

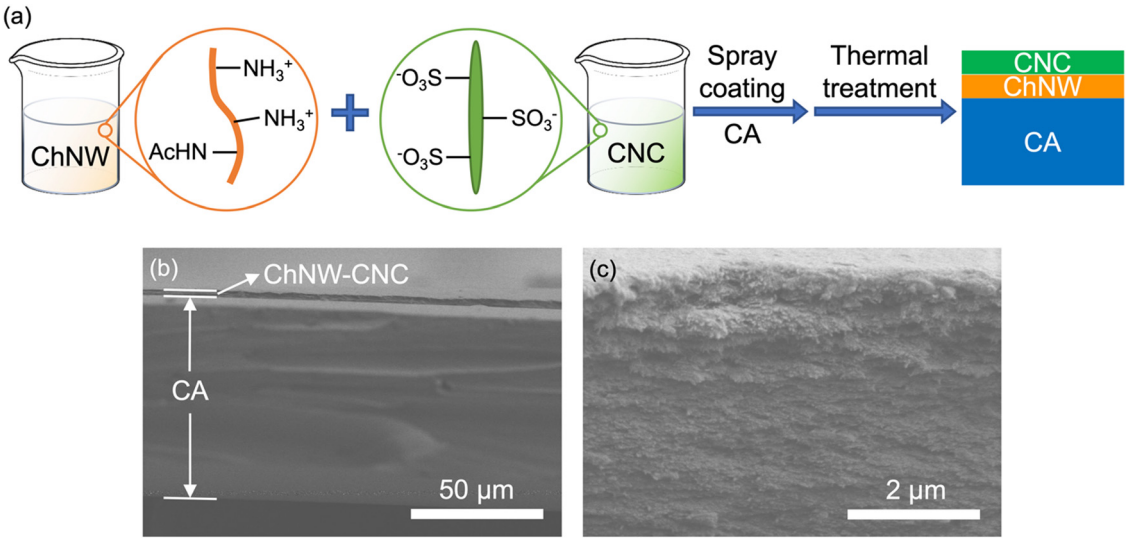

Fig. 1 (a) Schematic of the formation of a multilayer film: CA coated with ChNWs and CNCs. Cross-sectional SEM images for S80T40 sample (b) and its ChNW–CNC coating at a higher resolution (c).

content will result in more open interfibrillar interfaces and more capillary pores, which will increase oxygen transport through the film.[28] Though the coated film with a T_{spray} of 100 °C had the lowest OP, the film became observably yellow (as shown in the section of optical properties), which indicated oxidation of cellulose. Thus, in the following study on the influence of $T_{thermal}$ on film properties, the T_{spray} was controlled at 80 °C.

Similarly, by increasing the $T_{thermal}$ from 40 to 140 °C at a controlled T_{spray} of 80 °C, the OP of the coated film decreased from 27.3 ± 1.2 to 11.5 ± 0.9 cm^3 μm m^{-2} day^{-1} kPa^{-1} (Fig. 2b). Among them, only S80T120 and S80T140 had a lower OP than S80T*n* (*i.e.*, 21.4 ± 3.9 cm^3 μm m^{-2} day^{-1} kPa^{-1}). Nevertheless, an interesting finding is that unlike coated films sprayed at different temperatures, the values of moisture content in the coatings for S80T*n* and S80T40 to S80T140 samples did not show an obvious correlation with the $T_{thermal}$ (Fig. S3b, ESI†). This suggests that $T_{thermal}$ did not influence the hornification. It is likely because fiber mobility was limited in the absence of a solvent during post thermal annealing, which led to unchanged microstructure with different $T_{thermal}$ values. After thermal annealing, moisture is likely regained during sample conditioning. It was found that post drying thermal annealing did not significantly influence the total moisture content of a pre-dried hygroscopic material (*i.e.*, cotton) after the material was conditioned at a consistent temperature and RH (21 °C, 65% RH) until equilibrium.[29] In our work, samples after thermal treatment were conditioned identically by exposing films to ~53% RH at room temperature for at least 7 days, during which it is likely that all films with similar microstructures regained moisture to a similar extent. Since the ChNW–CNC coatings of samples treated at different $T_{thermal}$ all had similar moisture contents and densities, due to similar coating thicknesses

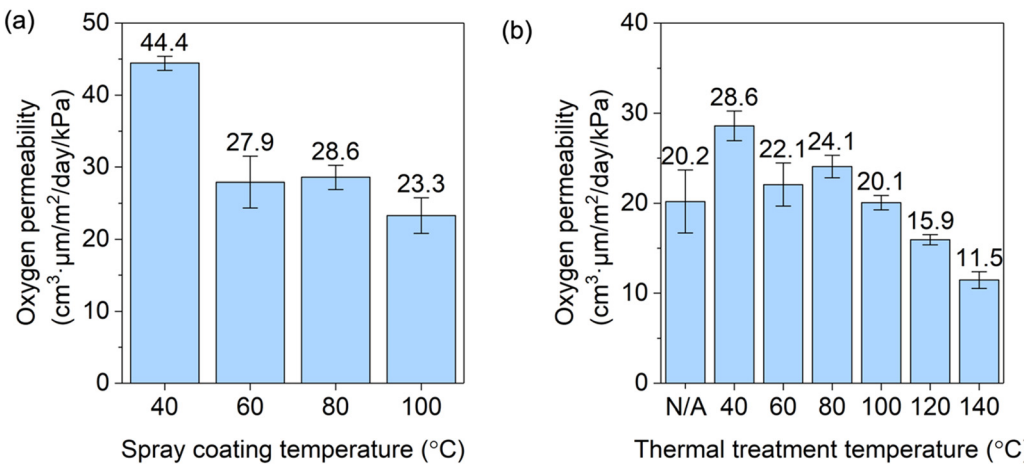

Fig. 2 Oxygen permeability values for coated films with different spray coating temperatures and a controlled thermal treatment temperature (40 °C) (a) and with different thermal treatment temperatures and a controlled spray coating temperature (80 °C) (b). 'N/A' represents sample S80T*n* without being thermally treated.

(Table 1) and similar applied coating mass per unit area of the film (*i.e.*, 5.6 ± 0.3 g m^{-2}), the decrease in the OP with an increasing $T_{thermal}$ is possibly attributed to other factors. For instance, it has been found that increasing the drying temperature of a free-standing CNF film increases its crystallinity.[9] An increase in crystallinity reduces the fiber flexibility and free-volume, and thus hinders the solubility and transport of O_2.[30]

The optimal sample (S80T140) with an OP of 11.5 ± 0.9 cm^3 μm m^{-2} day^{-1} kPa^{-1} showed an improvement in oxygen barrier property in comparison to previous studies utilizing similar materials. In our previous study where a bilayer of ChNWs and CNCs were spray coated on CA, the lowest OP was 16.7 cm^3 μm m^{-2} day^{-1} kPa^{-1} for a film with a T_{spray} of 65 °C with no thermal treatment.[22] This prior value is lower than that of S80T*n* in this study mainly because of different chitin sources and different purification processes, but higher than that of S80T140 because of the lack of post thermal treatment at a high temperature. In Satam *et al.*'s work, the coated film had up to five alternating layers of ChNF and CNC on PLA by spray coating at 60 °C without thermal treatment, and the OP values of the coated films ranged from 20 to 30 cm^3 μm m^{-2} day^{-1} kPa^{-1}.[23] Aside from the post thermal treatment, the reduced length and increased charge density (as indicated by a lower degree of acetylation shown in Table S2, ESI†) of ChNWs in our work also possibly resulted in a denser packing of the coating. Nevertheless, the optimal OP in our work was higher than those in some other previous studies. Some studies applied higher numbers of alternating thin layers of oppositely charged chitin- or cellulose-based nanomaterials as a gas barrier. For instance, Nguyen *et al.* deposited 20 bilayers of ChNW and TEMPO-oxidized CNF on both sides of polypropylene (PP) by dip coating and drying at 80 °C, resulting in an OP of 7.76 cm^3 μm m^{-2} day^{-1} kPa^{-1} at 23 °C and 50% RH.[19] Thuy *et al.* sprayed 40 bilayers of CsW and CNF on PET at 80 °C, followed by hot pressing, which had an OP of 0.91 cm^3 μm m^{-2} day^{-1} kPa^{-1} at 23 °C and 0% RH and 2.32 cm^3 μm m^{-2} day^{-1} kPa^{-1} at 60% RH.[21] Li *et al.* deposited up to 30 bilayers of chitosan and CNCs on PET by dip coating and the resulting film had an OP of ~2.4 cm^3 μm m^{-2} day^{-1} kPa^{-1} at 23 °C and 0% RH.[24] Kim *et al.* sprayed up to 50 bilayers of ChNW and CNF on PET, followed by hot pressing, and the sample with 20 bilayers had the lowest OP of 0.25 cm^3 μm m^{-2} day^{-1} kPa^{-1} at 23 °C and 0% RH.[20] The coatings in these studies have more interfaces between the oppositely charged materials and a higher thickness ratio of the interface to the bulk layer, which may result in a denser structure. However, the deposition of tens of layers adds to the process complexity, a trade-off for the barrier performance. Furthermore, many of these reported values were measured at 0% RH, rather than in humidified oxygen, and it is known that the OP values of cellulose, chitin, and their multilayers significantly increase with humidity.[21,28] Additionally, the use of a different substrate with oxygen barrier properties different from CA, such as PET and PP in the studies cited, also leads to the differences in OP of the coated film. While all these factors contribute to difficulties in making direct comparisons between the OP values measured in this study with previous reports, the OP of our highest performing film (*i.e.*, 11.5 ± 0.9 cm^3 μm m^{-2} day^{-1} kPa^{-1}) was significantly lower than those of many traditional plastics for food packaging, including polyethylene (PE), polystyrene (PS), PP, PVC, and PLA, as shown in Table S5 (ESI†).[23,31,32] It is comparable to the OP of the lowest reported values for commercially available PET (~10 cm^3 μm m^{-2} day^{-1} kPa^{-1}).[31] The normalized OTR for the S80T140 sample under atmospheric conditions (assuming 23 °C, 50% RH, 21 kPa of O_2 pressure as driving force, and 100 μm total film thickness) was 2.4 cm^3 m^{-2} day^{-1}. It satisfies the O_2 barrier requirements for some food products, such as fresh produce, bakery products, cheeses, meats, and peanuts.[28]

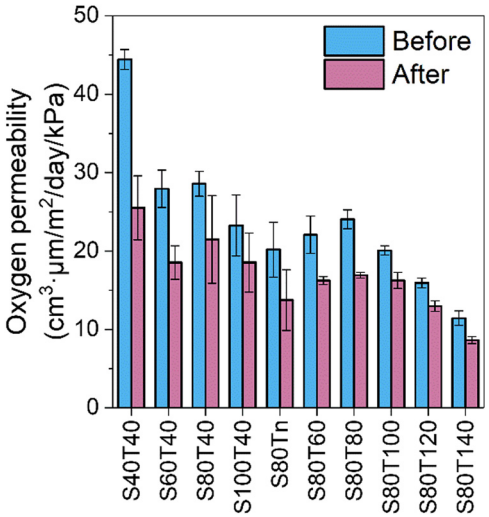

Fig. 3 Comparison of oxygen permeability values of coated films before (blue) and after (pink) six months of conditioning.

Another interesting finding is that the OP of all coated films decreased over time, while the overall trend that OP decreases with an increasing T_{spray} or $T_{thermal}$ did not change. A comparison of the original OP values and the OP values tested after another six months of conditioning at room temperature and ~53% RH is shown in Fig. 3. Generally, the samples with a relatively high original OP (*i.e.*, with a low T_{spray} or $T_{thermal}$) showed more significant decreases. One possible explanation is that the ChNWs and CNCs rearranged to form increasing numbers of inter-fiber hydrogen bonds during physical aging, which resulted in a decrease in the porosity of the coating. This was indicated by the density measurements of selected samples (Table S6, ESI†) where the average values of densities of S40T40 and S80T140 increased by 6% and 12%, respectively, after conditioning for another six months, although these changes were within the error bars. This improvement in oxygen barrier property over time suggests a long service life of the coated film as a packaging material.

Water vapor barrier property

The water vapor transmission rate (WVTR) values for the coated films are shown in Fig. 4. The WVTR values for coated films were on average 11% lower than that of a CA film (*e.g.*, 8.3 ± 0.1 g mm m^{-2} day^{-1}). The WVTR values for S40T40–S100T40

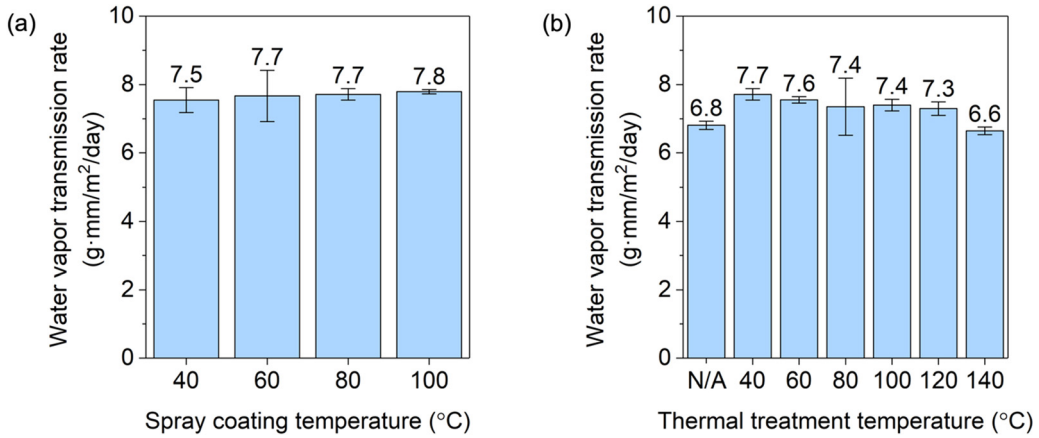

Fig. 4 Water vapor transmission rate values for coated films with different spray coating temperatures and a controlled thermal treatment temperature (40 °C) (a) and varying thermal treatment temperatures and a controlled spray coating temperature (80 °C) (b). 'N/A' represents sample S80T*n* without being thermally treated.

were not significantly influenced by T_{spray}, which is in contrast with the decrease in OP with increasing T_{spray}. It is likely that even though OP decreased, additional hornification is required in order to affect the solubility and diffusion of water. In fact, the moisture content decreased by only a small amount from 5.1% to 4.4% from the lowest to the highest T_{spray}. The WVTR values for coated films slightly decreased with an increasing $T_{thermal}$, which is also possibly attributed to increased crystallinity that limits fiber mobility and reduces free volume.[9] It has been found in a free-standing TEMPO-oxidized CNF film that the surface hydrophobicity can be enhanced by increasing $T_{thermal}$, which was correlated with the sorption of moisture.[33,34] In our study, however, the water contact angles on the CNC side of the coated films were not significantly affected by $T_{thermal}$, shown in Table S7 (ESI†). Thus, the increase in crystallinity is hypothesized to play a dominant role in improving the water vapor barrier property. The normalized WVTR for the S80T140 sample with the lowest OP under atmospheric conditions (assuming 23 °C, 50% RH, and 100 μm total film thickness) was 66 g m^{-2} day^{-1}. Though the film would benefit from further WVTR reduction for broader applications in food packaging, it meets the water vapor barrier requirement for packaging materials for fresh produce, bakery products, and cheese.[28]

However, this improvement in WVTR is limited in comparison to those in previous literature. For instance, it has been reported that the WVTR of a self-standing TEMPO-oxidized CNF film decreased by 84% by increasing the $T_{thermal}$ from 100 to 145 °C.[9] The thermal annealing time in the aforementioned work was longer than that in our work (*i.e.*, 3 h *versus* 1 h) and the ChNW–CNC was very thin in our work, which probably resulted in limited improvement in WVTR. The comparison in WVTR among the coated films in this work and commercial plastics for food packaging is shown in Table S5 (ESI†), and there remains large room for further improvement in WVTR of the coated film in this work. This could be achieved by applying a moisture barrier (*e.g.*, PP, PE, or poly(glycolic acid)) as a top layer,[6,31,35,36] introducing appropriate fillers (*e.g.*, nanoclay or metal oxide nanoparticles) to the coating,[37–39] promoting interparticle cross-linking,[40] or reducing the moisture content.[25] Thuy *et al.* applied two bilayers of silanized CsW and silica nanoparticles (CsW/SiO_2NP) on the uncoated side of PET film, where the other side was deposited with 40 bilayers of CsW and CNC. The CsW/SiO_2NP side was lubricated with oil, and the resulting film had a WVTR of 0.08 g mm m^{-2} day^{-1} which was 61% lower than those of the coated film without the CsW/SiO_2NP coating, respectively.[21] These methods will also be beneficial for improving the oxygen barrier property.

Mechanical properties

The coating of ChNW–CNC improved the mechanical properties in comparison to an untreated CA film, while interestingly adjusting the T_{spray} or $T_{thermal}$ did not significantly influence the mechanical properties, as shown in Table 2. Representative penetration–force curves obtained by puncture testing and stress–strain curves obtained by microtensile testing are available in Fig. S4 and S5 (ESI†) for coated films with different T_{spray} and $T_{thermal}$, respectively. Analyses on statistical

Table 2 Mechanical properties for untreated CA and coated samples

Sample	F_B[a] (N)	E[a] (GPa)	σ_y[a] (MPa)	ε_B[a] (%)
CA	38.5 ± 0.8	2.39 ± 0.25	42.9 ± 5.9	3.3 ± 1.0
S40T40	47.8 ± 2.0	2.44 ± 0.26	49.2 ± 3.9	8.9 ± 6.1
S60T40	45.6 ± 2.5	2.58 ± 0.13	47.8 ± 1.7	8.7 ± 6.1
S80T40	47.6 ± 3.4	2.62 ± 0.22	49.9 ± 4.3	5.5 ± 3.3
S100T40	46.1 ± 4.3	2.45 ± 0.12	50.5 ± 1.5	14.5 ± 5.3
S80T*n*	47.7 ± 2.3	2.87 ± 0.10	57.2 ± 5.0	3.4 ± 0.9
S80T60	41.6 ± 2.3	2.81 ± 0.05	53.3 ± 1.4	3.5 ± 0.4
S80T80	44.0 ± 1.3	2.82 ± 0.09	53.8 ± 2.0	10.4 ± 6.4
S80T100	45.2 ± 1.3	2.78 ± 0.07	53.6 ± 2.4	6.6 ± 3.0
S80T120	47.9 ± 1.6	2.71 ± 0.14	53.2 ± 2.2	3.9 ± 0.4
S80T140	45.9 ± 2.1	2.73 ± 0.22	52.3 ± 7.4	11.3 ± 7.9

[a] The breaking force (F_B) was measured by puncture testing (ASTM F1306). The modulus (E), yield stress (σ_y), strain at break (ε_B) values were obtained by microtensile testing (ASTM D1708).

significance for the mechanical properties are available in Tables S8–S11 (ESI†), where mechanical properties for treated CA films (*i.e.*, CAS40–CAS100, and CAT40–CAT140) are shown in Table S12 (ESI†).

For coated films with different T_{spray} (S40T40–S100T40) or $T_{thermal}$ (S80T40–S80T140), the breaking force values were on average 21% and 18% higher than that of untreated CA, respectively. This difference is attributed to the increased film thickness (*i.e.*, 76 μm for the uncoated film and 79–80 μm for the coated films) and the coating of ChNWs and CNCs. However, the values of modulus, yield stress, and strain at break for different T_{spray} values generally showed no significant difference from those of the untreated CA. For coated films with different $T_{thermal}$, the strain at break values were also not significantly different from that of the untreated CA, but the values of modulus and yield stress were on average 15% and 23% higher than those of the untreated CA film, respectively. The S80T*n* sample had the highest values of modulus (2.87 ± 0.10 GPa) and yield stress (57.2 ± 5.0 MPa) among the coated films, but these were not significantly different from those of S80T60 to S80T140. Differences in the mechanical properties were generally insignificant with varying T_{spray} or $T_{thermal}$, separately. This is mainly because the coating took up only ~5% of the total film thickness, and the mechanical properties of the coated films were dominated by the substrate, rather than processing temperatures. Furthermore, the data in Table S12 (ESI†) show that the mechanical properties of the CA samples treated with spray coating of water or thermal treatment separately were not significantly influenced by adjusting the T_{spray} or $T_{thermal}$. However, the properties of these treated samples were enhanced relative to those obtained for the bare CA. Since these mechanical property measurements were collected sometime after those for the CA and coated CA films, this property difference may be related to changes in the substrate that are occurring with time, as was reported for the OP measurements in Fig. 3. Detailed discussion of the mechanical properties of treated CA films is shown in the ESI.† Overall, processing parameters may be adjusted to enhance gas barrier properties without large sacrifices in mechanical properties. The modulus and yield stress values of the coated films here, dominated by those of the CA substrate, were comparable to or superior to those of many common plastics for food packaging, including PE, PS, PP, PVC, PLA, PET, and EVOH,[41] as shown in Table S13 (ESI†), even though the strain at break values were lower. Thus, the coated films in this work satisfy the mechanical property requirement for packaging applications.

Optical properties

Photographs of the untreated CA and all coated films are shown in Fig. 5a. Qualitatively, with the exception of S100T40, which had a slight yellow color, the film color was not affected by the various thermal treatments. Quantitatively, we observed a distinct trend in optical properties, specifically the transmittance and the haze of the films, as a function of the T_{spray} and $T_{thermal}$,

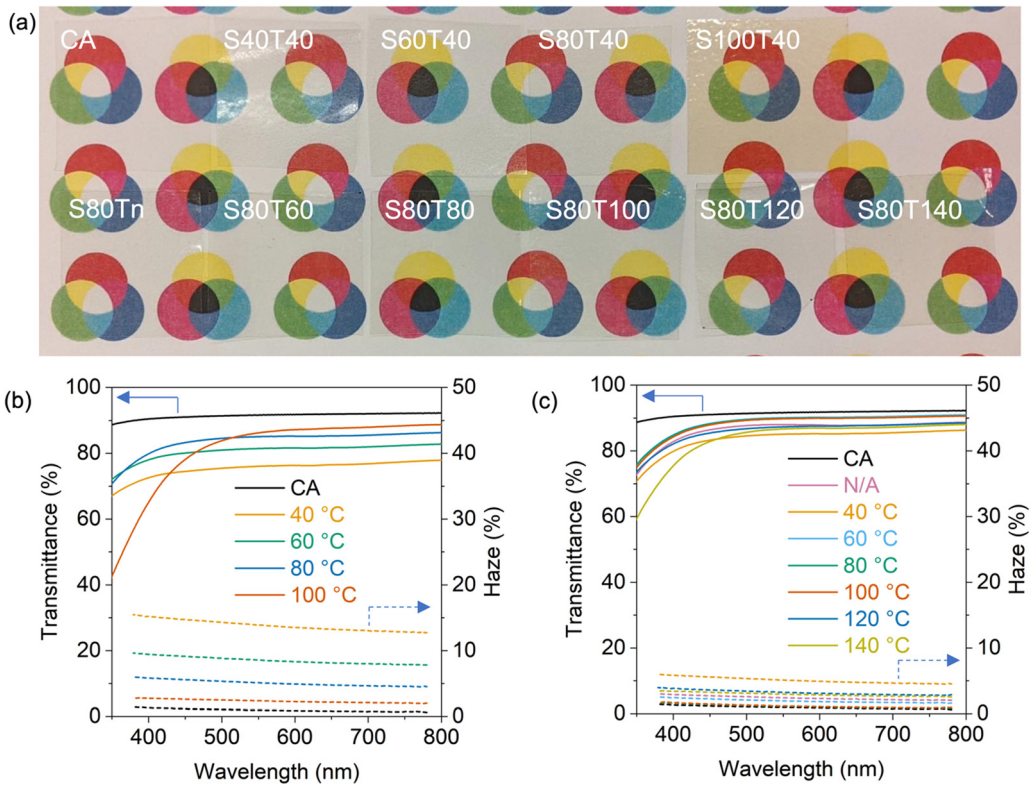

Fig. 5 Photographs (a), transmittance (solid line) and haze (dash line) spectra (b and c) for uncoated CA and coated films with different spray coating temperature (b) and different thermal treatment temperature (c). 'N/A' in c represents sample S80T*n* without being thermally treated.

as shown in Fig. 5b and c. Throughout the visible spectrum (380–780 nm) as T_{spray} increased, the transmittance increased from an average of 75% transmittance for S40T40 to 81% transmittance for S100T40, and the haze decreases from an average of 13% to 2%. Given the lack of chromophores that would absorb light throughout the visible spectrum in any of the layers, we attribute the enhancement in the transmissivity largely to a decrease in the haze. This trend in haze likely resulted from different surface textures formed by different rates of liquid droplet drying during surface coating. At lower T_{spray}, the longer times required for liquid droplets to dry appear to lead to larger wetting ridges and substrates becoming rougher, giving rise to more light scattering;[42] conversely, higher T_{spray} leads to decreased drying times and smoother films with less scattering. This is observed in both optical microscope images (Fig. S6, ESI†) as well as a decrease in surface roughness determined by profilometry (Fig. S7, ESI†). The change in refractive index (RI) differences between CNC and ChNW or between ChNW and CA with temperature may also account for this change in transmittance and haze. It has been found that a smaller difference in RIs for two materials results in a lower haze.[43] For instance, it has been found that the RIs for cellulose and chitin are $\sim$1.54 and $\sim$1.56, respectively.[44,45] At a higher temperature, the RI for cellulose increases while that for chitin decreases,[46,47] so the RI difference between CNC and ChNW likely decreases with an increasing temperature, which may cause an decrease in haze. A decrease in transmittance at shorter wavelengths was especially pronounced for S100T40. Previous studies on free-standing ChNF and CNC films have observed absorbance in the UV tailing into the visible spectrum caused by light absorption of amide in ChNWs (at $\sim$230 nm) and sulfate ester groups in CNCs (at $\sim$270 nm),[48–50] and the decrease in transmittance for S100T40 was attributed to keto or carboxyl groups formed by the oxidation of hydroxyl groups.[51] Due to the notable yellowing at higher temperatures, the upper limit of T_{spray} was selected to be 100 °C.

For S80T*n* and films with different $T_{thermal}$, the relationship between $T_{thermal}$ and optical properties is more complex (Fig. 5c). A slight increase in transmittance and a decrease in haze is again observed with increasing temperatures between 40 °C and 80 °C, however at higher temperatures the transmittance decreases while the haze increases. The notable drop in transmittance at shorter wavelengths for S80T140 also suggested the oxidation of hydroxyl groups.[51] In spite of these changes, the transmittance remains above 80% and the haze below 4% for all $T_{thermal}$ values, suggesting that the surface morphology is mostly established during spray coating; this is corroborated by the relatively lower surface roughness measured for all films with different $T_{thermal}$ compared to T_{spray} (Fig. S7, ESI†). The samples annealed at 80 °C and 100 °C attain average transmittance values of 88–89% and a haze of 1% across the visible spectrum, nearly approaching the optical performance of CA films (92% transmittance and 1% haze). A comparison in optical properties between the coated film in this work and commercial materials for food packaging is shown in Table S14 (ESI†). The high transmittance and low haze of our bilayer films support their use in potential applications such as electronic device packaging as well as food packaging.[52]

Conclusions

In this work, we show a simple method to improve the oxygen barrier property of a renewably sourced bio-based multilayer film by increasing the processing temperatures. A bilayer of ChNWs and CNCs was spray-coated on CA. The OP of a coated film was decreased 48% and 62% by increasing the T_{spray} from 40 to 100 °C and by increasing the $T_{thermal}$ (post thermal annealing) from 40 to 140 °C, respectively. The optimal sample in this work had gas barrier properties that meet the requirements for the packaging of many types of food products. We also report for the first time that the OP of this polysaccharide-based multilayer film decreased over time. The coated films also had enhanced mechanical properties and water vapor barrier properties and maintained high transmittance and low haze in comparison to the untreated CA film, and these properties were not significantly influenced by T_{spray} or $T_{thermal}$. These properties all make the CA film coated with a bilayer of ChNWs and CNCs a potential renewable substitute for petroleum-based plastics for food and other barrier packaging applications.

Although the oxygen barrier, mechanical, and optical properties of the coated films in this work satisfy the requirements for packaging of some types of food, there remains large room for improving the water vapor barrier property due to the hydrophilic nature of polysaccharides. Besides, there are other properties that are significant for the industrial production of food packaging materials and need further investigation and improvement for coated films in this work, including heat-sealing properties, grease barrier property, printability, *etc.* Though such properties can usually be improved by other functional layers, it adds to the complexity and cost for industrial production, and the functional layers are mostly non-biodegradable materials. Thus, how to improve these properties for renewable biodegradable materials is still a problem for future exploration.

Conflicts of interest

M. L. S. is serving as a guest editor for the themed collection on Biomass Materials to be published in Materials Advances.

Acknowledgements

The authors acknowledge the Department of Energy (DOE) for financial support of this work (EE0008494). Y. J. acknowledges Prof. Victor Breedveld for assistance with rheological measurements of the suspensions. This work was performed in part at the Georgia Tech Institute for Electronics and Nanotechnology,

a member of the National Nanotechnology Coordinated Infrastructure (NNCI), which is supported by the National Science Foundation (ECCS-2025462).

References

1 G. L. Robertson, *Food Packaging: Principles and Practice*, Taylor & Francis Group, Bosa Roca, United States, 3rd edn, 2012.
2 J. W. Rhim, H. M. Park and C. S. Ha, *Prog. Polym. Sci.*, 2013, **38**, 1629–1652.
3 M. J. Kirwan, S. Plant and J. W. Strawbridge, in *Food and Beverage Packaging Technology*, ed. R. Coles and M. Kirwan, Wiley-Blackwell, Oxford, 2011, pp. 157–212, DOI: **10.1002/9781444392180.ch7**.
4 A. Chamas, H. Moon, J. J. Zheng, Y. Qiu, T. Tabassum, J. H. Jang, M. Abu-Omar, S. L. Scott and S. Suh, *ACS Sustainable Chem. Eng.*, 2020, **8**, 3494–3511.
5 V. Siracusa and I. Blanco, *Polymers*, 2020, **12**, 1641.
6 Z. Y. Yu, Y. Ji, V. Bourg, M. Bilgen and J. C. Meredith, *Emergent Mater.*, 2020, **3**, 919–936.
7 S. Ifuku and H. Saimoto, *Nanoscale*, 2012, **4**, 3308–3318.
8 R. J. Moon, A. Martini, J. Nairn, J. Simonsen and J. Youngblood, *Chem. Soc. Rev.*, 2011, **40**, 3941–3994.
9 J. Y. Xia, Z. Zhang, W. Liu, V. C. F. Li, Y. F. Cao, W. Zhang and Y. L. Deng, *Cellulose*, 2018, **25**, 4057–4066.
10 C. C. Satam, C. W. Irvin, C. J. Coffey, R. K. Geran, R. Ibarra-Rivera, M. L. Shofner and J. C. Meredith, *Biomacromolecules*, 2020, **21**, 545–555.
11 J. Wu, K. Zhang, N. Girouard and J. C. Meredith, *Biomacromolecules*, 2014, **15**, 4614–4620.
12 T. H. Zhong, M. P. Wolcott, H. Liu and J. W. Wang, *Carbohydr. Polym.*, 2019, **226**, 115276.
13 B. Duan, C. Y. Chang, B. B. Ding, J. Cai, M. Xu, S. C. Feng, J. Z. Ren, X. W. Shi, Y. M. Du and L. N. Zhang, *J. Mater. Chem. A*, 2013, **1**, 1867–1874.
14 P. Bordes, E. Pollet and L. Averous, *Prog. Polym. Sci.*, 2009, **34**, 125–155.
15 E. Csiszar and S. Nagy, *Carbohydr. Polym.*, 2017, **174**, 740–749.
16 I. Kelnar, J. Kovarova, G. Tishchenko, L. Kapralkova, E. Pavlova, F. Carezzi and P. Morganti, *J. Polym. Res.*, 2015, **22**, 5.
17 T. H. Tran, H.-L. Nguyen, D. S. Hwang, J. Y. Lee, H. G. Cha, J. M. Koo, S. Y. Hwang, J. Park and D. X. Oh, *Carbohydr. Polym.*, 2019, **205**, 392–400.
18 R. A. Chowdhury, M. Nuruddin, C. Clarkson, F. Montes, J. Howarter and J. P. Youngblood, *ACS Appl. Mater. Interfaces*, 2019, **11**, 1376–1383.
19 H. L. Nguyen, T. H. Tran, L. T. Hao, H. Jeon, J. M. Koo, G. Shin, D. S. Hwang, S. Y. Hwang, J. Park and D. X. Oh, *Carbohydr. Polym.*, 2021, **271**, 118421.
20 T. Kim, T. H. Tran, S. Y. Hwang, J. Park, D. X. Oh and B. S. Kim, *ACS Nano*, 2019, **13**, 3796–3805.
21 V. T. T. Thuy, L. T. Hao, H. Jeon, J. M. Koo, J. Park, E. S. Lee, S. Y. Hwang, S. Choi, J. Park and D. X. Oh, *Green Chem.*, 2021, **23**, 2658–2667.
22 Y. Ji, S. Waters, E. Lim, A. W. Lang, P. N. Ciesielski, M. L. Shofner, J. R. Reynolds and J. C. Meredith, *ACS Sustainable Chem. Eng.*, 2022, **10**, 124–133.
23 C. C. Satam, C. W. Irvin, A. W. Lang, J. C. R. Jallorina, M. L. Shofner, J. R. Reynolds and J. C. Meredith, *ACS Sustainable Chem. Eng.*, 2018, **6**, 10637–10644.
24 F. Li, P. Biagioni, M. Finazzi, S. Tavazzi and L. Piergiovanni, *Carbohydr. Polym.*, 2013, **92**, 2128–2134.
25 S. Sharma, X. D. Zhang, S. S. Nair, A. Ragauskas, J. Y. Zhu and Y. L. Deng, *RSC Adv.*, 2014, **4**, 45136–45142.
26 S. E. M. Selke and J. D. Culter, in *Plastics Packaging*, ed. S. E. M. Selke and J. D. Culter, Hanser, 3rd edn, 2016, pp. 353–393, DOI: **10.3139/9783446437197.014**.
27 L. Salmen and J. S. Stevanic, *Cellulose*, 2018, **25**, 6333–6344.
28 J. Wang, D. J. Gardner, N. M. Stark, D. W. Bousfield, M. Tajvidi and Z. Cai, *ACS Sustainable Chem. Eng.*, 2018, **6**, 49–70.
29 F. R. Andrews, E. Honold and J. N. Grant, *Text. Res. J.*, 1963, **33**, 609–616.
30 E. A. McGonigle, J. J. Liggat, R. A. Pethrick, S. D. Jenkins, J. H. Daly and D. Hayward, *Polymer*, 2001, **42**, 2413–2426.
31 J. Lange and Y. Wyser, *Packag. Technol. Sci.*, 2003, **16**, 149–158.
32 J. Muller, C. Gonzalez-Martinez and A. Chiralt, *Eur. Polym. J.*, 2017, **95**, 56–70.
33 W. S. Yang, Y. Gao, C. Zuo, Y. L. Deng and H. Q. Dai, *Carbohydr. Polym.*, 2019, **223**, 115050.
34 S. Belbekhouche, J. Bras, G. Siqueira, C. Chappey, L. Lebrun, B. Khelifi, S. Marais and A. Dufresne, *Carbohydr. Polym.*, 2011, **83**, 1740–1748.
35 C. Johansson, J. Bras, I. Mondragon, P. Nechita, D. Plackett, P. Simon, D. G. Svetec, S. Virtanen, M. G. Baschetti, C. Breen, F. Clegg and S. Aucejo, *BioResources*, 2012, **7**, 2506–2552.
36 K. J. Jem and B. Tan, *Adv. Ind. Eng. Polym. Res.*, 2020, **3**, 60–70.
37 S. H. Park, H. S. Lee, J. H. Choi, C. M. Jeong, M. H. Sung and H. J. Park, *J. Appl. Polym. Sci.*, 2012, **125**, E675–E680.
38 S. Amjadi, S. Emaminia, S. H. Davudian, S. Pourmohammad, H. Hamishehkar and L. Roufegarinejad, *Carbohydr. Polym.*, 2019, **216**, 376–384.
39 M. P. Indumathi, K. S. Sarojini and G. R. Rajarajeswari, *Int. J. Biol. Macromol.*, 2019, **132**, 1112–1120.
40 H. J. Wu, Y. L. Lei, J. Y. Lu, R. Zhu, D. Xiao, C. Jiao, R. Xia, Z. Q. Zhang, G. H. Shen, Y. T. Liu, S. S. Li and M. L. Li, *Food Hydrocolloids*, 2019, **97**, 105208.
41 MatWeb: Online Materials Information Resource, **https://www.matweb.com**, accessed 2022-05-05.
42 Z. Y. Cai, A. Skabeev, S. Morozova and J. T. Pham, *Commun. Mater.*, 2021, **2**, 1–11.
43 W. Wildner and D. Drummer, *ISRN Opt.*, 2014, **2014**, 802369.
44 H. L. Leertouwer, B. D. Wilts and D. G. Stavenga, *Opt. Express*, 2011, **19**, 24061–24066.
45 I. Niskanen, T. Suopajärvi, H. Liimatainen, T. Fabritius, R. Heikkilä and G. Thungström, *J. Quant. Spectrosc. Radiat. Transfer*, 2019, **235**, 1–6.

46 Z. Montiel-González, G. Luna-Bárcenas and A. Mendoza-Galván, *Phys. Status Solidi C*, 2008, **5**, 1434–1437.
47 I. Niskanen, K. Zhang, M. Karzarjeddi, H. Liimatainen, S. Shibata, N. Hagen, R. Heikkilä, H. Yoda and Y. Otani, *J. Polym. Res.*, 2022, **29**, 187.
48 Y. C. Peng and B. Via, *Polymers*, 2021, **13**, 2168.
49 S. Mujtaba Karim and R. Samuel, *Proc. - Indian Acad. Sci., Sect. A*, 1934, **1**, 398–406.
50 E. B. Nielsen and J. A. Schellman, *J. Phys. Chem.*, 1967, **71**, 2297–2304.
51 K. Ahn, S. Zaccaron, N. S. Zwirchmayr, H. Hettegger, A. Hofinger, M. Bacher, U. Henniges, T. Hosoya, A. Potthast and T. Rosenau, *Cellulose*, 2019, **26**, 429–444.
52 A. W. Lang, Y. Ji, A. C. Dillon, C. C. Satam, J. C. Meredith and J. R. Reynolds, *ACS Sustainable Chem. Eng.*, 2021, **9**, 2937–2945.